## PAPER

Check for updates

# Enhancing the mechanical performance of poly(ether ether ketone)/zinc oxide nanocomposites to provide promising biomaterials for trauma and orthopedic implants

Linlin Hao,[b] Ying Hu,[a] Yu Zhang,[b] Wenzhen Wei,[b] Xiaochen Hou,[a] Yiqiao Guo,[a] Xiyu Hu[a] and Dong Jiang [ID] *[a]

Poly(ether ether ketone)/zinc oxide (PEEK/ZnO) composites were manufactured by using the injection molding technique. Before blending with the PEEK resin matrix, some ZnO nanoparticles were modified by γ-aminopropyltriethoxylsilane (APTES). The effect of surface modification of ZnO nanoparticles by amino groups and Si–O bonds was investigated. PEEK/ZnO composites were characterized by scanning electron microscopy (SEM), thermogravimetric analysis, and X-ray diffraction. The scanning electron micrographs showed that ZnO nanoparticles were encapsulated in the PEEK phase; within this phase, the nanoparticles were homogeneously dispersed. Mechanical and tribological properties were measured by tensile strength, flexural strength, coefficient of friction, and wear rate. It was shown that the interfacial compatibility between ZnO nanoparticles and PEEK matrix was significantly enhanced due to the amino and Si–O bonds decorated on the ZnO nanoparticles. More importantly, the thermal stability of PEEK improved upon the incorporation of ZnO nanoparticles into this matrix. Cell viability studies with mouse osteoblasts demonstrated that cell growth on PEEK and PEEK/ZnO was significantly enhanced. On the basis of the obtained results, PEEK/ZnO composites are recommended as promising candidates for orthopaedic materials and trauma implants.

## Introduction

PEEK is a semi-crystalline colorless thermoplastic polymer with outstanding thermal stability, good mechanical properties and wear resistance, high glass transition temperature, *etc.* Due to such excellent properties, PEEK is widely used in aerospace industry, automotive industry, mechanical industry, medical and electronic applications, and many other fields.[1–5] The friction and wear properties of PEEK and its composites have been extensively studied.[6–15] Moreover, PEEK has no toxicity, solvent resistance, and can be repeatedly sterilized using conventional methods such as those employing steam, gamma radiation, and ethylene oxide without evident degradation of the mechanical properties.[16] Due to these particular properties, PEEK polymers can be used for long-term orthopaedic, cardiovascular, and dental implants. Importantly, experimental measurements have highlighted that the unfilled matrix of PEEK can undergo elastoplastic deformation.[17,18] Hence, many researchers have

attempted to engineer these materials with respect to their applications, particularly load-bearing orthopedic applications, in the biomedical field.[19–21] Sarasua *et al.* have earlier reported about the improvement in the mechanical properties of PEEK reinforced by short glass (GF-PEEK) and carbon fiber (CF-PEEK).[22] The composites were prepared by the injection molding approach and by using a maximum fiber loading of 30% by weight. Pace *et al.* reported a CF-PEEK composite acetabular cup that was implanted in the body, and it was analyzed using the histologic technique.[23] It was found that the wear depth in the retrieved insert was 0.130 mm at 28 months, and it was localized in the area of maximum wear, offset from the cup pole. Scolozzi *et al.* have reported PEEK for maxillary reconstruction; the patient was monitored for more than 5 years, and no complications were observed during this period, indicating that PEEK is an excellent biocompatible material with promising applications in reconstructive medicine.[24] Apart from CF and GP, other materials including phosphate[25] and nanosized hydroxyapatite[26–28] were used to make bioactive PEEK composites. All these materials meet the functional requirements for implant materials; thus, they can be used as replacements for human bone.

ZnO nanoparticles are multifunctional inorganic nanoparticles, and they exhibit excellent performances. ZnO

*[a]Engineering Research Center of High Performance Plastics, Ministry of Education, College of Chemistry, Jilin University, Qianjin Street 2699, Changchun 130012, People's Republic of China. E-mail: jiangdonghxy@163.com; Fax: +86 431 85168886; Tel: +86 431 85168886*

*[b]College of Animal Science, Jilin University, Xian Road 5333, Changchun 130062, People's Republic of China*

nanoparticles, which have high temperature resistance, good thermal conductivity, and low expansion coefficient, can significantly improve the chemical and mechanical stability of the material when they are used as reinforcing fillers.[29,30] Furthermore, ZnO nanoparticles are believed to be nontoxic, biosafe, low-cost and biocompatible. For all these reasons, ZnO nanoparticles have also been used as drug carriers, in cosmetics, and as fillers in other medical materials.[31]

It is worth pointing out that ZnO exhibits intensive ultraviolet absorption and significant antibacterial activity at pH values in the range of 7–8 even in the absence of light. Hence, ZnO is widely used for optical devices and antimicrobials.[32] Ana M. Díez-Pascual *et al.*[33,34] studied antimicrobials of PEEK/ZnO nanocomposites; they observed that the antibacterial activity of PEEK/ZnO nanocomposites against *Escherichia coli* and *Staphylococcus aureus* enhanced with the increasing ZnO content, and the best antibacterial property was obtained at 7.5 wt% of modified nanoparticles.

This study aims to investigate the potential of PEEK/ZnO composites as human bone substitutes suitable for load-bearing functions, and the wear resistance of PEEK is improved by the addition of ZnO particles without reducing its mechanical properties. PEEK–ZnO composites are prepared with a twin-screw extruder. The tensile properties, long-term durability and preliminary *in vitro* biological analysis are presented. The results of the cell viability test and cell differentiation indicate that these new nanocomposites have great potential as biomaterials for orthopaedic and trauma implants.

## Experimental

### 1. Materials

PEEK fine powders (Table 1) with a diameter of approximately 100 μm were prepared in Jilin University of China; ZnO nano-powder with <30 nm particle size and specific surface area ≥ 60 m² g⁻¹ was supplied by Nanjing Guanye Industry Chemicals Co., LTD. Ethanol (EtOH, 95.0%) was purchased from Beijing Chemical Reagent (China). APTES was purchased from Nanjing Fine Chemicals Co., LTD (China).

### 2. Preparation of surface-modified ZnO nanoparticles (m-ZnO)

ZnO nanoparticles were added into deionized water and heated under reflux for 3 h, and this procedure was repeated for 3 times. After filtration, the nanoparticles were dried at 100 °C for 12 h to remove the absorbed water. The surface-modified nanoparticles were obtained through the reaction between hydroxyl groups on the ZnO surface and the ethoxyl groups of APTES. In a typical protocol, a certain quantity of APTES was mixed with EtOH and stirred for 1 h. Glacial acetic acid was used to adjust the pH, which ranged between 5 and 6. Then, ZnO nanoparticles were added to the mixture solution. The resulting suspension was subjected to ultrasonication. Subsequently, the suspension was refluxed at 78 °C for 4.5 h. Finally, the modified nanoparticles were rinsed several times with EtOH to remove the excess of coupling agent and afterwards, they were dried in an oven at 80 °C. The resulting material was denoted as m-ZnO.

### 3. Preparation of PEEK/ZnO composites

PEEK resin, ZnO and m-ZnO were dried in an oven at 100 °C for 10 h to remove moisture. These materials, in a well-established weight ratio, were mixed in a high-speed mixer. The compositions of the composite materials are listed in Table 2. Furthermore, the mixed composites were combined using a HAAKE PTW16/25p (USA) co-rotating twin-screw extruder with a screw speed of 120 rpm. The temperature profiles of the barrel were 330/340/355/360/355/340 °C from the hopper to the dye. Subsequently, the strip samples were cut into granules and

**Table 1** Properties of PEEK

Mechanical data

| Tensile strength (MPa) | Tensile elongation (%) | Flexural strength (MPa) | Flexural modulus (GPa) |
| --- | --- | --- | --- |
| 95 | 58.4 | 141 | 3.5 |

Thermal data

| Melting point (°C) | Coefficient of thermal expansion (ppm °C⁻¹) | Heat deflection temperature (°C) | Thermal conductivity (W m⁻¹ °C⁻¹) |
| --- | --- | --- | --- |
| 339 | 55 | 152 | 0.3 |

Miscellaneous

| Density (g cm⁻³) | Melting viscosity (Pa s) | Volume resistivity (Ω cm) | Friction coefficient (mm³ N⁻¹ m⁻¹) | Friction loss (mm³ N⁻¹ m⁻¹) | Melt index g/10 min |
| --- | --- | --- | --- | --- | --- |
| 1.32 | 450 | $10^{15}$ | 0.48 | $5.5 \times 10^{-6}$ | 85 |

Table 2  ZnO nanoparticles/PEEK composites ratio

| Samples | ZnO (wt%) | PEEK (wt%) |
|---|---|---|
| ZnO/PEEK | 2.5 | 97.5 |
| ZnO/PEEK | 5.0 | 95.0 |
| | m-ZnO (wt%) | PEEK (wt%) |
| m-ZnO/PEEK | 2.5 | 97.5 |
| m-ZnO/PEEK | 5.0 | 95.0 |
| m-ZnO/PEEK | 7.5 | 92.5 |
| m-ZnO/PEEK | 10.0 | 90.0 |

dried in an oven at 120 °C for 4 h. Then, PEEK composites were injected with HAAKE MiniJet II (HAAKE, Germany) for molding different shapes of testing bars. The standard tests in bars were injected at a barrel temperature of 380 °C and a mold temperature of 180 °C. The three kinds of bars were used for tensile tests, three-point flexural tests, and friction tests (Fig. 1).

## 4.  Characterization

**FTIR spectroscopy.** Infrared spectrum was obtained using a Nicolet Impact 410 Fourier Transform Infrared (FTIR) spectrophotometer. The test conditions were 4000–400 cm$^{-1}$ scanning range, resolution of 4 cm$^{-1}$, and 128 acquisitions per spectrum. A mixture of sample and KBr was tested.

**X-ray diffractometry (XRD).** The crystalline structures of PEEK and PEEK/ZnO composites were characterized with an X-ray diffractometer (XRD, Rigaku D/Max 2550 X-ray Diffractometer, Japan) using CuKα radiation operated at 200 mA and 50 kV.

**Thermogravimetric analysis (TGA).** TGA was performed on a Perkin Elmer Pyris-1 thermo-gravimetric analysis instrument,

USA. The samples were heated from 100 to 800 °C with a heating rate of 10 °C min$^{-1}$ under 20 mL min$^{-1}$ nitrogen flow.

**Differential scanning calorimetry (DSC).** The crystallization behaviors of the composites were determined with TA Q2000 DSC Instruments (USA). The composites were first heated from 80 to 400 °C with a heating rate of 10 °C min$^{-1}$, and the temperature was maintained at 400 °C for 5 min. Next, cooling scans were performed from 400 to 80 °C with a cooling rate of 10 °C min$^{-1}$; after that, new heating scans were carried out from 80 to 400 °C with a speed of 10 °C min$^{-1}$. The crystallization temperature ($T_c$) and crystallization enthalpy ($\Delta H_c$) were determined on the first cooling scan, whereas the melting temperature ($T_m$) was obtained on the second heating scan.

**Thermo-mechanical analysis (TMA).** The linear expansion coefficients of PEEK and PEEK/ZnO composites were determined with TMA/SDTA841e (METTLER TOLEDO, Switzerland). The PEEK and PEEK composites were heated from 40 to 200 °C with a heating rate of 10 °C min$^{-1}$.

**Mechanical tests.** The tensile and three-point flexural tests were performed with AG-120KN (SHIMADZU, Japan) at room temperature with speeds of 5 and 2 mm min$^{-1}$, respectively.

**Tribological experiments.** Tribological experiments were performed with a pin-on-disc apparatus friction testing machine (UMT-2, Center For Tribology Inc., Campbell, CA, USA). The apparent pressure was 1 MPa, and the sliding velocity was 200 rpm with a test time of 2 h.

**Scanning electron microscopy (SEM).** The morphologies of ZnO, m-ZnO, PEEK, and PEEK/ZnO composites were characterized with SEM (FEI Nova Nano 450 FEI, field emission SEM system, USA) at an accelerating voltage of 15 kV.

**Transmission electron microscopy (TEM).** TEM was performed using a Hitachi H-800 electron microscope at an acceleration voltage of 200 kV with a CCD camera. High-angle annular dark-field scanning TEM energy-dispersive X-ray
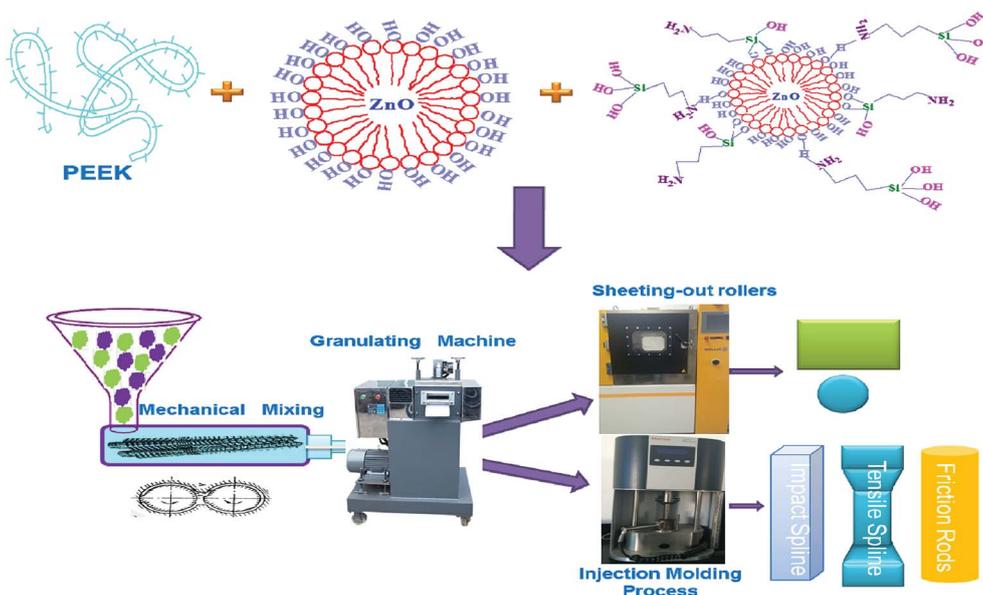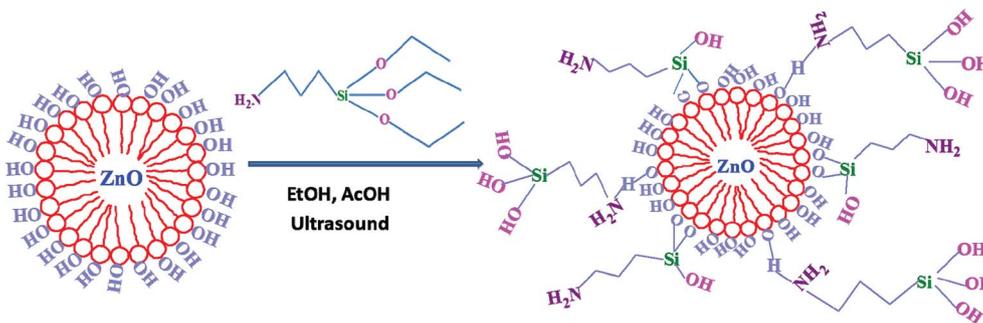


Fig. 1  The preparation flow chart of PEEK composite.

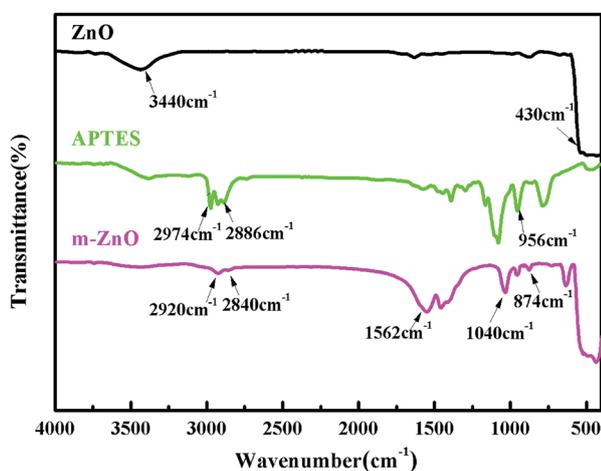Scheme 1   Preparation of modified zinc oxide nanoparticles.



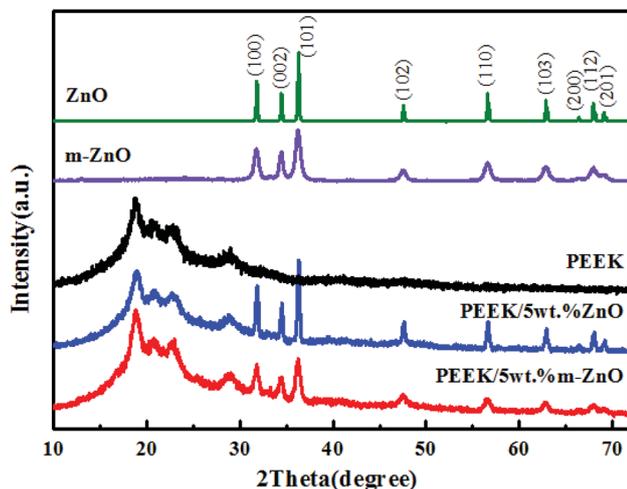Fig. 2   Spectra of ZnO, functionalized ZnO, and APTES.



Fig. 3   XRD patterns of ZnO and PEEK composites.

spectroscopy (HAADF-STEM-EDS) was conducted with a FEI Tecnai F20 transmission electron microscope at 200 kV.

**Cell culture.** Mouse osteoblasts (MC3T3-E1), provided by Professor Zhang Yan's laboratory (Key Laboratory of Gene Engineering of the Ministry of Education, Sun Yat-sen

University, China), were cultured in DMEM medium (Gibco Co., New York, NY, USA) containing 10% fetal bovine serum (FBS), 3% $NAHCO_2$, 100 U $mL^{-1}$ penicillin, and 100 µg $mL^{-1}$ streptomycin at 37 °C with 5% $CO_2$ in a humidified incubator. After reaching 80% confluence, the cells were trypsinized and counted with a hemocytometer. The PEEK and PEEK/ZnO composites were cut into small slices and placed in a cell culture plate, followed by sterilization under ultraviolet radiation for 2 h. The cells were seeded onto membranes of PEEK and PEEK composites ($n = 3$) at a density of $1 \times 10^5$ cell per mL.

Cell viability on membranes of PEEK and PEEK/ZnO composites was determined by the MTT (3-(4,5-dimethylthiazol-2-yl)-2,5-diphenyltetrazolium bromide) method (Beyotime Biotechnology, Jiangsu, China). Briefly, the cell and membranes of PEEK and PEEK/ZnO composites were incubated with 100 µL Cell-Titer 96 Aqueous One Solution Reagent containing MTT for 4 h. The absorbance of the supernatant was measured at 570 nm.

Morphological studies of *in vitro*-cultured MC3T3-E1 on membranes of PEEK and PEEK/ZnO composites were performed. Initially, the membranes incubated with cells were taken out after 3 days and washed three times with PBS (phosphate-buffered sodium) to remove unattached cells. The cells were then fixed with 4% formaldehyde water solution for 2 h, dehydrated in a graded concentration series of ethanol (10, 30, 50, 70, 90, 95, and 100%), and finally freeze-dried. After coating with gold, the samples were observed using scanning electron microscopy (SEM, S-3400 N Japan Hitachi Co., Ltd., Tokyo, Japan) at an accelerated voltage of 2 kV.

**Alkaline phosphatase (ALP) activity.** For osteogenic differentiation assay, MC3T3-E1 cells were seeded at a density of 1.0 $\times 10^4$ cells per $cm^2$ on PEEK and PEEK/ZnO composites. One day after the cells were seeded, the medium was replaced with a differentiation medium α-DMEM (Gibco) with 10% FBS, 1% penicillin/streptomycin, 50 µg $mL^{-1}$ ascorbic acid (Sigma Aldrich), 10 mM β-glycerophosphate phosphate (Sigma Aldrich) and 10 nM dexamethasone (Sigma Aldrich). Cells of the eight groups of treatment were collected from each well at different time points and assayed for ALP activity. Each component ALP activity was determined using a commercially available ALP kit (Nanjing Jiancheng Biotech Co., Ltd) according to standard procedures. The 24-well plate (Croning) was washed three times with PBS; then, 200 µL of 0.1% Triton X-100 was added to lyse
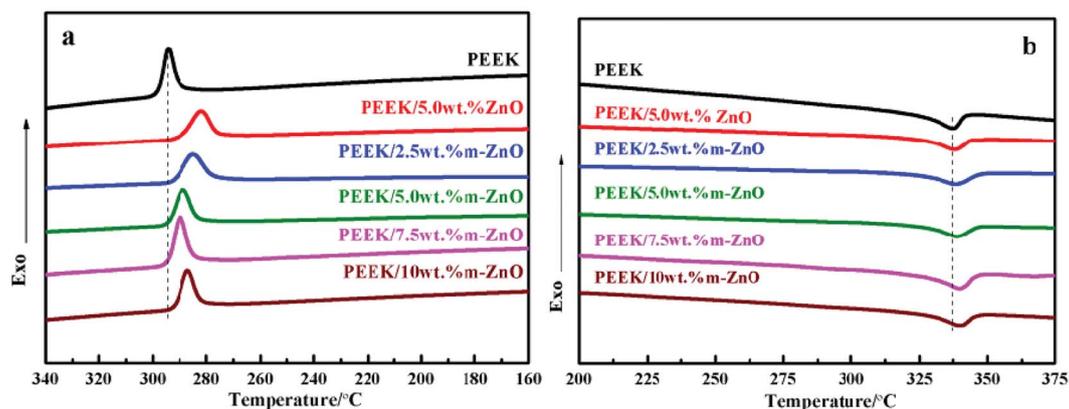
**Fig. 4** Non-isothermal DSC cooling (a) and heating (b) scans of PEEK and the PEEK–ZnO nanocomposites with different nanoparticle loadings.

**Table 3** Thermal parameters obtained from DSC analysis of PEEK and the nanocomposites reinforced with raw or modified ZnO (*) nanoparticles

| ZnO (wt%) | 0 | 5.0 | 2.5* | 5.0* | 7.5* | 10.0* |
|---|---|---|---|---|---|---|
| $T_c$ (°C) | 294 | 282 | 285 | 289 | 290 | 287 |
| $T_m$ (°C) | 338 | 338 | 339 | 339 | 340 | 339 |
| $X_c$ (%) | 24.5 | 25.7 | 26.6 | 27.2 | 27.1 | 25.3 |

**Table 4** Thermal parameters obtained from TGA analysis of PEEK and the nanocomposites reinforced with raw or modified ZnO (*) nanoparticles

| ZnO (wt%) | 0 | 2.5 | 2.5* | 5.0 | 5.0* | 10.0* |
|---|---|---|---|---|---|---|
| $T_5$ (°C) | 572 | 576 | 576 | 578 | 580 | 583 |
| $T_{10}$ (°C) | 582 | 585 | 585 | 588 | 590 | 592 |



**Fig. 5** TGA curves obtained under a nitrogen atmosphere for PEEK and the corresponding nanocomposites.



**Fig. 6** DTG curves of PEEK and its composites.

**Table 5** CTE of PEEK and PEEK composites

| Sample | PEEK | PEEK/2.5 wt% m-ZnO | PEEK/5.0 wt% m-ZnO | PEEK/10 wt% m-ZnO |
|---|---|---|---|---|
| CTE (ppm K$^{-1}$) | 104 | 103 | 101 | 99 |

the cells for 30–40 minutes and subsequently, the reaction reagents were added according to the manufacturer's recommendations. Finally, the ALP absorbance was measured at 520 nm using a microplate reader (Tecan Auatria GmbH). Protein concentration was measured at 595 nm using a protein assay reagent (Beyotime Bradford Protein Assay Kit) according to the manufacturer's instructions, and the level of ALP activity was normalized by the amount of total protein.

## Results and discussion

### 1. FTIR characterization of m-ZnO

The surface of ZnO was treated with APTES, as shown in Scheme 1. Aminosilane coupling agent reacted with ZnO through various interactions including the hydroxyl surface groups of the ZnO nanoparticles and the $-OCH_2CH_3$ groups of the coupling agent *via* a substitution reaction. The FTIR spectra of

**Table 6** The mechanical properties of PEEK and its composites

| Sample | Tensile strength (MPa) | Strain at break (%) | Flexural strength (MPa) | Young's modulus (GPa) |
|---|---|---|---|---|
| PEEK | 95 | 54 | 136 | 1.8 |
| PEEK/5.0 wt% ZnO | 97 | 45 | 137 | 2.0 |
| PEEK/2.5 wt% m-ZnO | 97 | 50 | 137 | 2.0 |
| PEEK/5.0 wt% m-ZnO | 98 | 49 | 138 | 2.1 |
| PEEK/7.5 wt% m-ZnO | 101 | 48 | 143 | 2.1 |
| PEEK/10 wt% m-ZnO | 99 | 48 | 139 | 2.1 |

ZnO, m-ZnO, and APTES are displayed in Fig. 2 to prove the success of ZnO modification. In the spectrum of ZnO, a broad peak could be observed at 3440 cm$^{-1}$, thus confirming the presence of OH groups on the nanoparticle surface. Furthermore, an intense peak appeared at 430 cm$^{-1}$, and it corresponded to the stretching of Zn–O bonds. In the spectrum of APTES, an evident peak could be observed at 956 cm$^{-1}$, which confirmed the presence of Si–O groups. The spectrum of m-ZnO revealed some new peaks as compared to that of ZnO. The bands at 2920 and 2840 cm$^{-1}$ were assigned to symmetrical and asymmetrical stretching vibrations of C–H in CH$_3$ and CH$_2$ groups, respectively. Furthermore, the peak at 1040 cm$^{-1}$ was assigned to Si–O–Si asymmetric stretching, whereas that at 874 cm$^{-1}$ was due to the symmetrical stretching vibrations of Zn–O–Si. In addition, a new band appeared at around 1562 cm$^{-1}$, and it was assigned to the bending vibration of the N–H deformation mode that shifted to a lower wavenumber due to the interaction with silanol groups or surface hydroxyl groups of ZnO. The appearance of these bands proved that the functional groups in APTES were successfully attached on the surface of ZnO nanoparticles.[35–38]

## 2. XRD characterization

Fig. 3 shows the XRD patterns of ZnO and m-ZnO nanoparticles over the 2$\theta$ range of 10–70°. The pattern of ZnO shows characteristic peaks at 2$\theta$ values of 31.8°, 34.4°, 36.2°, 47.6°, 56.6°, 62.9°, 66.4°, and 67.9°, which correspond to the diffractions of the (100), (002), (101), (102), (110), (103), (112), and (201) crystalline planes. All the diffraction peaks can be well indexed to hexagonal ZnO (JCPDS card no. 36-1451). The high purity of the synthesized nanoparticles is confirmed through the well-defined diffraction peaks and no sign of impurities. The modified ZnO nanoparticles display an almost identical pattern as that of the unmodified nanoparticles, but the results differ mainly in the width and intensity of some peaks. However, it is worth mentioning that the coupling agent has no influence on the crystalline structure of ZnO nanoparticles. Fig. 3 also shows the diffractogram of a semi-crystalline PEEK polymer; this diffractogram displays characteristic peaks at 2$\theta$ values of 18.8°, 20.7°, 22.9°, and 28.9°, which correspond to the diffractions of (110), (111), (200), and (211) crystalline planes. On the basis of these two reference diffractograms, the diffractogram registered for the PEEK/ZnO composite materials is carefully analyzed; we establish that it displays the characteristic diffraction peaks of the two components, clearly demonstrating the successful

incorporation of ZnO into the PEEK matrix. However, as can be observed in Fig. 3, the intensity and width of the peaks in the diffractogram of PEEK/ZnO composites are lower than those of PEEK. This indicates that the addition of nanoparticles can change the spherulite's size of PEEK.

## 3. Crystalline and melting behaviors of composite materials

In special engineering plastics, poly(ether ether ketone) is a semi-crystalline polymer material. The crystallization and melting behaviors of a composite material strongly affect the properties of composite materials. To evaluate these effects, the thermal analysis data of PEEK/ZnO nanocomposites were obtained under non-isothermal conditions by the DSC technique. The obtained results are illustrated in Fig. 4 and Table 3.

From Table 3, it can be seen that the crystallization temperature ($T_c$) of the PEEK/ZnO nanocomposites was lower than that of PEEK, but the melting temperature ($T_m$) and crystallinity ($X_c$) were higher than those of PEEK. The decrease in $T_c$ was mainly due to the use of ZnO nanoparticles as nucleating agents, which constrained PEEK to crystallize at a lower temperature. For the composites with m-ZnO nanoparticles, the crystallization temperature, melting temperature and crystallinity increased with the increase in m-ZnO, but a descending trend appeared when the concentration of nanoparticles was higher. The $X_c$ value of the 5.0 wt% m-ZnO composite was the highest, but the $X_c$ value of the sample containing 10 wt% m-ZnO was lower. This result can be due to the fact that m-ZnO
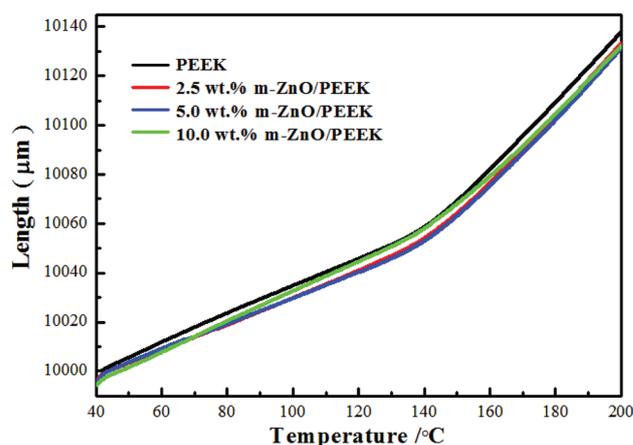


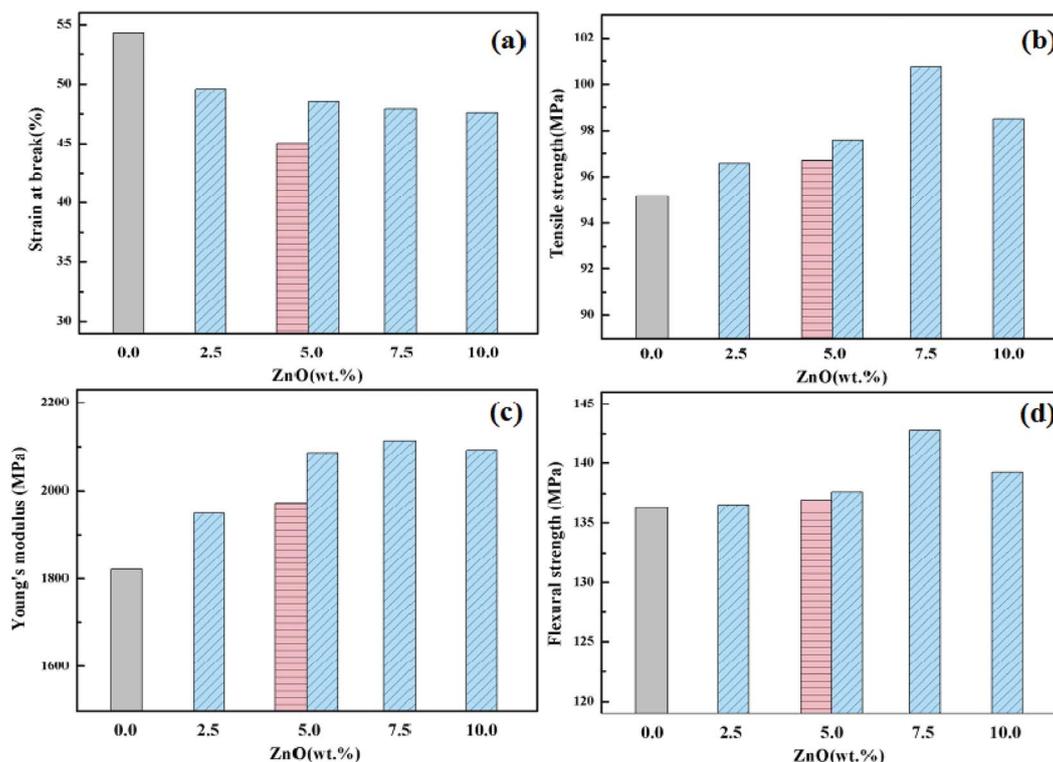**Fig. 7** TMA curves of PEEK and PEEK composites.

**Fig. 8** Comparison of the mechanical properties of PEEK–ZnO nanocomposites with different nanoparticle loadings: (a) strain at break; (b) tensile strength; (c) Young's modulus; (d) flexural strength. The pink and blue bars correspond to composites reinforced with ZnO or m-ZnO.

species are regarded as heterogeneous nuclei in PEEK crystallization. The modified nanoparticles were homogeneously dispersed in the composite matrix, and the nucleating centers became larger in size; thus, crystallinity improved. However, at higher concentrations, the strong interaction between the nanoparticles might impose restrictions on PEEK chain diffusion and crystal growth. Therefore, the crystallinity of the composite decreased. A similar situation was observed in PEEK–SWCNT composites mixed with polysulfones that are used as compatibilizing agents.[39]

### 4. Thermal properties of composite materials

Fig. 5 shows the thermal weight loss curves of PEEK and its composites under a nitrogen atmosphere. The characteristic degradation temperatures of all composite samples are presented in Table 4. From the graphs and table, it can be seen that the thermal stability of composites containing oxide nanoparticles was higher than that of PEEK. The decomposition of PEEK started at the temperature of 528 °C, and the sample exhibited the maximum rate of weight loss at approximately 585 °C; at 800 °C, the residual mass was around 51% of its initial weight. As shown in Table 4, the values of $T_5$ and $T_{10}$ increased with the increase in the content of nanoparticles. When the content of ZnO was 5.0 wt%, $T_5$ and $T_{10}$ increased by 6 and 5 °C, respectively, compared with those for PEEK. However, when the amount of m-ZnO was 5.0 wt%, $T_5$ and $T_{10}$ of the composites were further enhanced. When the content of m-ZnO was 10 wt%, $T_5$ and $T_{10}$ increased by nearly 10 °C compared with

those for PEEK. This can be ascribed to the barrier effect of the well-dispersed nanoparticles, which effectively hindered the diffusion of degradation products from the bulk of the matrix to the gas phase.[40] Moreover, the high thermal conductivity of ZnO facilitated heat dissipation within the composite, thus resulting in enhanced thermal stability.[41] This result was in agreement with that of derivative thermogravimetric analysis (DTG), for which the curves are displayed in Fig. 6. When the temperature was below 524 °C, the weight loss rates of all samples remained consistent, and the decomposition of PEEK played the
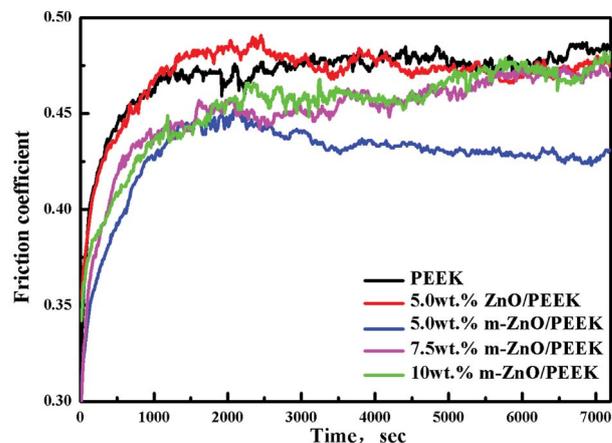


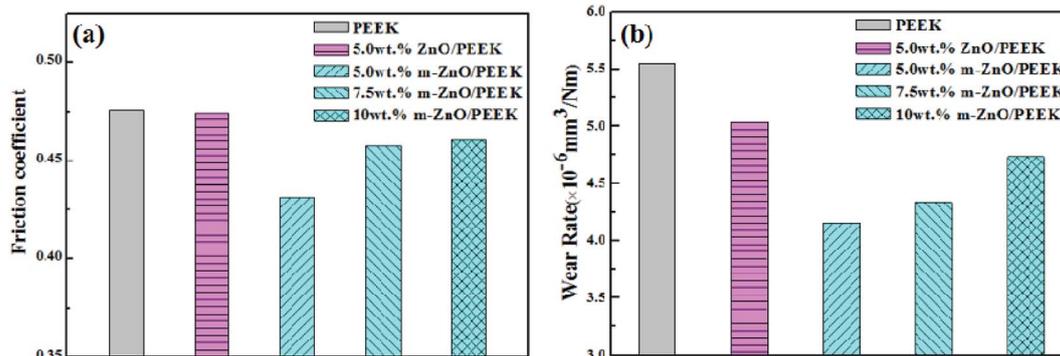**Fig. 9** The curves of the friction coefficients of PEEK and its composites.

**Fig. 10** Tribological properties of PEEK–ZnO nanocomposites and PEEK: (a) friction coefficient; (b) wear rate.

dominant role. Above 524 °C, the decomposition of PEEK resulted in change in the weight loss rate of the PEEK composites (Table 5).

## 5. The dimensional stability of composite materials

Dimensional stability stipulates that the size of the material does not change under mechanical, thermal or other external stress. Therefore, the linear expansion coefficient of the prepared materials was measured to emphasize their ability to retain the size regardless of the environmental conditions. The test results of the thermo-mechanical analysis are listed in

Table 5, whereas the linear expansion coefficient curves are shown in Fig. 7. As can be seen from figure and table, the linear expansion coefficients of the PEEK composites decreased with the increase in m-ZnO content, which was mainly due to the low coefficient of linear expansion of zinc oxide. These results confirmed that the addition of ZnO improves the dimensional stability of the composite material.

## 6. Mechanical properties of composite materials

The mechanical properties of PEEK and its composites prepared by adding different amounts of ZnO and m-ZnO,
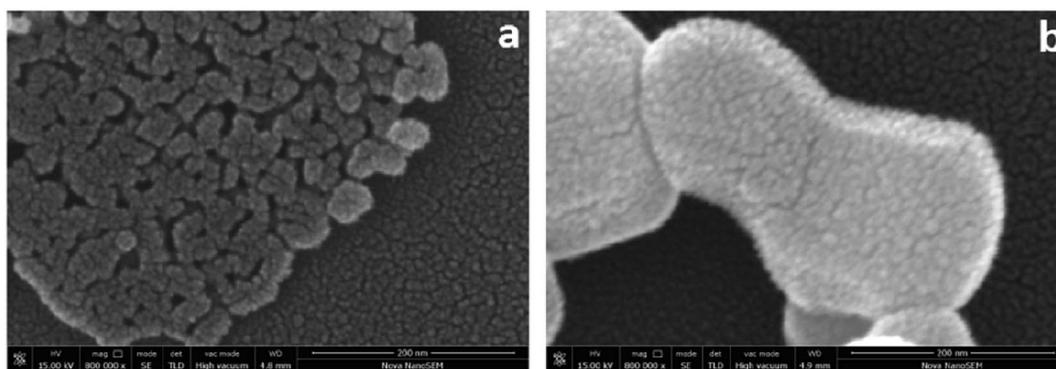


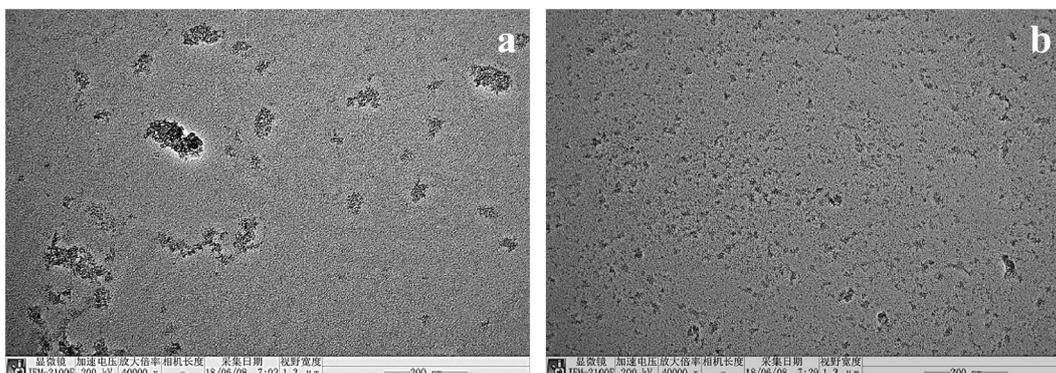**Fig. 11** Typical SEM micrographs of surface (a) ZnO and (b) m-ZnO.



**Fig. 12** TEM images of PEEK/ZnO (a) 5 wt% ZnO/PEEK (b) 5 wt% m-ZnO/PEEK.
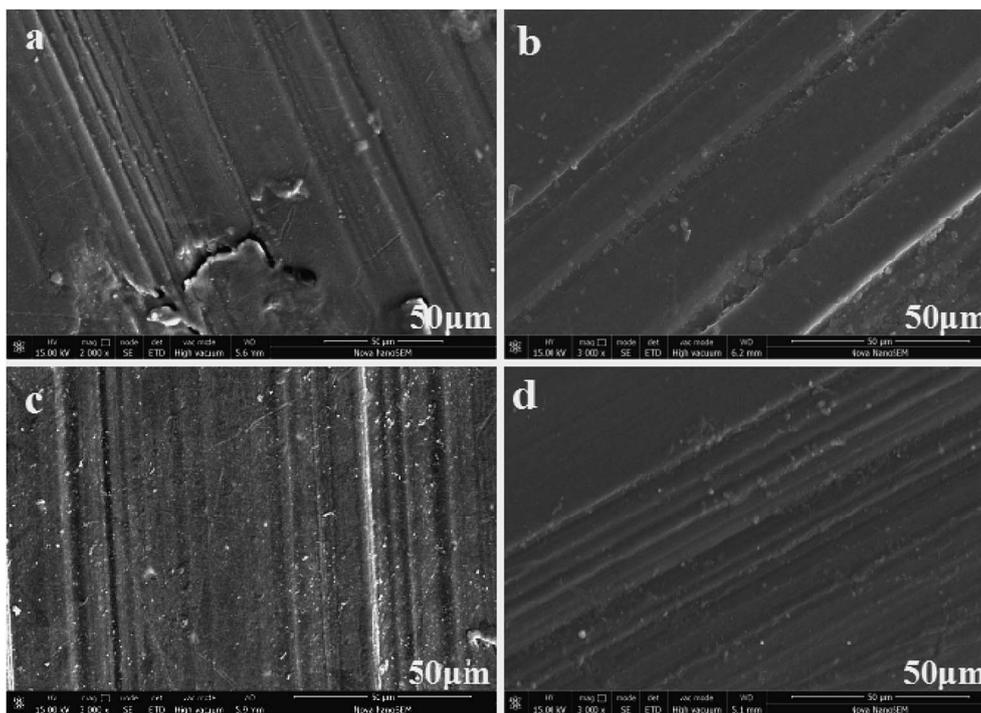
Fig. 13   Worn surfaces of PEEK and PEEK composite materials, (a) PEEK, (b) 5 wt% ZnO/PEEK, (c) 5 wt% m-ZnO/PEEK, (d) 7.5 wt% m-ZnO/PEEK.

respectively, are shown in Table 6 and Fig. 8. It can be seen in Table 6 and Fig. 8 that the tensile strength, flexural strength and Young's modulus of the nanocomposites were higher than those of PEEK, whereas the elongation at break was lower. When the content of m-ZnO was 7.5 wt%, the flexural strength, Young's modulus and tensile strength were 143 MPa, 2.1 GPa, and 101 MPa, respectively. Hence, it is evident that the addition of ZnO nano-particles enhanced the mechanical properties of the composites, but the improvement was not very significant. This probably is due to the small size of the nanoparticles and the fact that the PEEK matrix resin bears the main external stress. The mechanical properties of the modified nano-particle composites were better than those of the composites obtained by directly adding pure nanoparticles, which may be due to the addition of the coupling agent to enhance the compatibility between the nanoparticles and PEEK. The nanoparticles were dispersed more uniformly and reduced the stress concentration.[42]

## 7.  Friction and wear behavior of composite materials

It is well-known that inorganic nanoparticles can improve the friction and wear behaviors of polymers. However, these effects are related to the microstructure of the composites and the size, shape, and type of the inorganic nanoparticles as well as the degree of dispersion of the particles. Fig. 9 shows that the curves of friction coefficients of PEEK and its composites as a function of the test conditions were at 200 °C min$^{-1}$ and a load of 1 MPa at room temperature. It can be seen from Fig. 9 that at the initial stages, the friction coefficient rapidly increased; then, it decreased slowly and stabilized.

Fig. 10 illustrates the histograms of the friction coefficient (a) and the wear rate (b) of PEEK and its composites. The coefficient of friction of PEEK was about 0.48; for the sample containing 5.0 wt% ZnO, the value was close to the value of PEEK. In contrast, when the same content of m-ZnO was added to the PEEK matrix material, the friction coefficient was the lowest; then, it increased with the increase in the m-ZnO content. The results showed that 5.0 wt% of m-ZnO is the optimum amount of filler to obtain the maximum strength of such a nanocomposite. The wear rate of PEEK was 5.54 × 10$^{-6}$ mm$^3$ N$^{-1}$ m$^{-1}$. After adding 5 wt% m-ZnO in the PEEK matrix material, the wear rate was reduced by about 25%; however, with the increase in m-ZnO content, the wear rate started to increase. In contrast, the wear rate of the composites filled with m-ZnO decreased to a greater extent, which was mainly due to the addition of the coupling agent; this improved the degree of dispersion of the nano-particles, thus improving the adhesion between m-ZnO nano-particles and resin. In addition, the friction between the material and the dual surface contact area reduced sliding friction. With the increase in wear time, the surface temperature of friction increased, whereas the dispersed nanoparticles could inhibit plastic deformation of matrix materials. Therefore, the friction coefficient of composites containing the modified nanoparticles was lower. For the composites loaded with the lowest amount of modified nanoparticles, a rough surface appeared between the friction surface and the dual disc in the process of sliding friction. In addition, the rigid nano-particles played the role of a ball in the process of friction while playing a role in supporting the load, which reduced the contact area in the friction process, thereby reducing the friction coefficient and wear rate.[43]
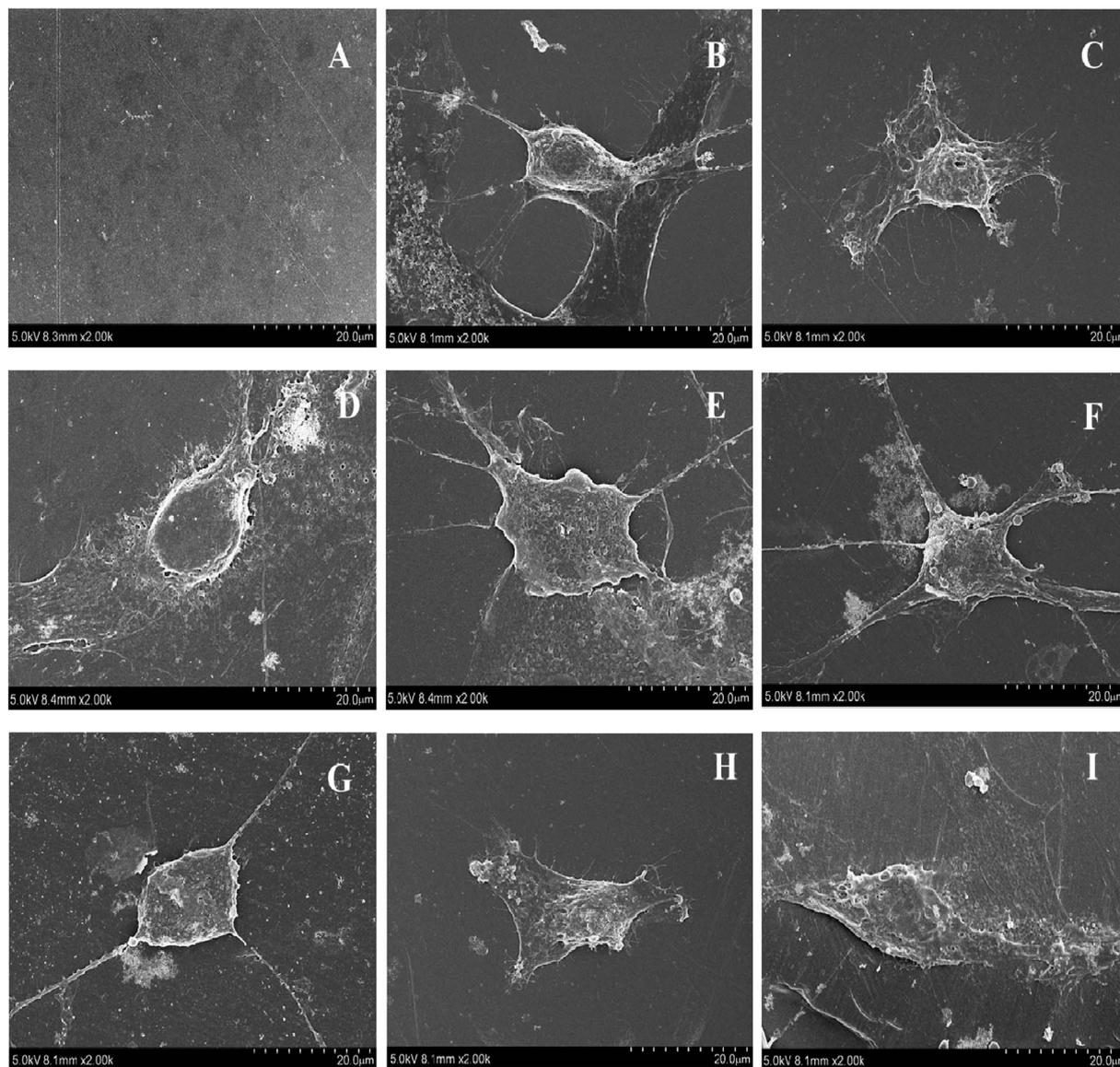
**Fig. 14** Mouse osteoblasts on membranes of PEEK and PEEK/ZnO composites after 3 days, (A) PEEK without cell, (B) cell on microslide, (C) cell on PEEK, (D) cell on PEEK/2.5 wt% ZnO, (E) cell on PEEK/5.0 wt% ZnO, (F) cell on PEEK/2.5 wt% m-ZnO, (G) cell on PEEK/5.0 wt% m-ZnO, (H) cell on PEEK/7.5 wt% m-ZnO, (I) cell on PEEK/10 wt% m-ZnO.

In summary, it can be stated that the rational design of PEEK–inorganic nanoparticle composites can provide new nanomaterials with excellent wear-resistance.

## 8. Morphological analysis of ZnO nanoparticles

The SEM images of ZnO and m-ZnO are shown in Fig. 11. It can be observed in Fig. 11(a) that most of the ZnO nanoparticles were agglomerated into an irregular shape due to their high surface energy and large specific surface area. The m-ZnO particles were clear and well dispersed, as seen in Fig. 11(b). The above-mentioned results proved that APTES was grafted onto the surface of ZnO. These improved morphological properties are explained by the silane molecules that provide

spatial repulsion between m-ZnO nanoparticles, thus preventing their aggregation.

## 9. Morphological analysis of composite materials

The dispersion of ZnO nanoparticles within PEEK was also analyzed by TEM. The micrographs of the composite materials of 5 wt% ZnO/PEEK and 5 wt% m-ZnO/PEEK are shown in Fig. 12(a) and (b), respectively. Clearly, the surface-treated nanoparticles were more uniformly distributed within PEEK, which was in agreement with SEM observations. The addition of APTES reduced the aggregation of the nanoparticles, promoted their interfacial adhesion with PEEK, and enhanced the mechanical and tribological performances of the composite materials.
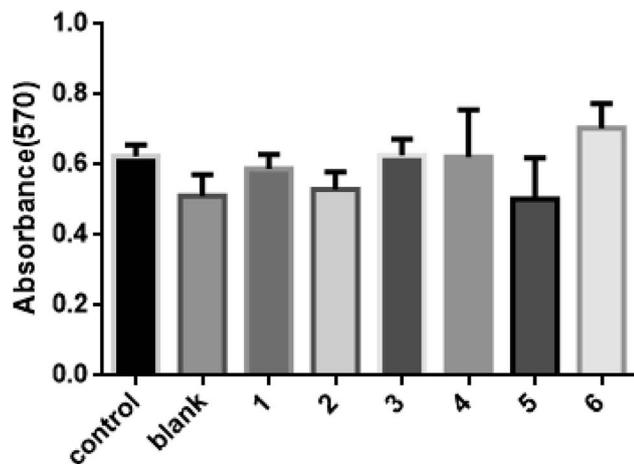
**Fig. 15** MTT results for MC3T3-E1 on membranes of PEEK and PEEK/ZnO composites after 3 days of cell culture (*$P$ 0.05), blank: PEEK, 1: PEEK/2.5 wt% ZnO, 2: PEEK/5.0 wt% ZnO, 3: PEEK/2.5 wt% m-ZnO, 4: PEEK/5.0 wt% m-ZnO, 5: PEEK/7.5 wt% m-ZnO, 6: PEEK/10 wt% m-ZnO.

## 10. Morphological analysis of worn surface

Fig. 13 shows the microstructure of the wear surface of PEEK and its composites. It can be observed in Fig. 13(a) that numerous furrows and wiredrawing phenomenon appear on the friction and wear surface of PEEK. Moreover, there were evident scratches and a small amount of abrasive dust on its surface; this was observed because PEEK has lower interface shear strength and thus, it can be easily pulled off to form worn debris. Fig. 13(b)–(d) display the morphologies of the composites with different ZnO nanoparticles; it can be seen from these figures that the wear mechanism changed to abrasive wear-based and had a slight adhesion wear. This might be due to the addition of ZnO, which improved the shear strength and hardness of the interface, reduced the amount of abrasive

debris, and reduced the scavenging effect of debris on the friction surface during the friction process. In contrast, the wear of the friction surface for 5 wt% ZnO in composite (c) was relatively low. Although the surface appeared furrowed, it was shallower, and the surface was relatively flat. Because of the addition of m-ZnO, which could be uniformly dispersed in the raw material, the concentration of stress, plastic deformation of the surrounding materials and plastic flow were reduced.

## 11. Cell morphology and viability

In this study, the adhesion and proliferation of MC3T3-E1 onto membranes of PEEK and PEEK/ZnO composites were determined. The results from SEM observation are presented in Fig. 14. The cells adhered well on the surface of all membranes. More cells were significantly clustered around the membranes. Fig. 15 shows the viability of cells cultured on the membranes of PEEK and PEEK/ZnO composites determined by using the MTT method. No cytotoxicity was detected on the first day upon the loading of the membrane with the cultured cells. Furthermore, no significant difference between the PEEK and PEEK/ZnO composites ($P$ 0.05) was observed although the cell proliferation on blend membranes of PEEK/ZnO exhibited a slightly higher value.

## 12. Cell differentiation

In the experiment, the ALP activity of MC3T3-E1 on PEEK and PEEK/ZnO composite membranes was determined, which is the effect of the composite membrane on the differentiation of MC3T3-E1 cells. The results in Fig. 16 show that the ALP activity of the cultured cells on the membrane is time-dependent. As the culture time increased, the ALP activity also gradually increased. In addition, no significant difference was observed in the ALP activities of the cells grown on PEEK and PEEK/ZnO composites ($P < 0.05$) although the cell ALP activity on the PEEK/ZnO blend membrane was higher than that of the PEEK
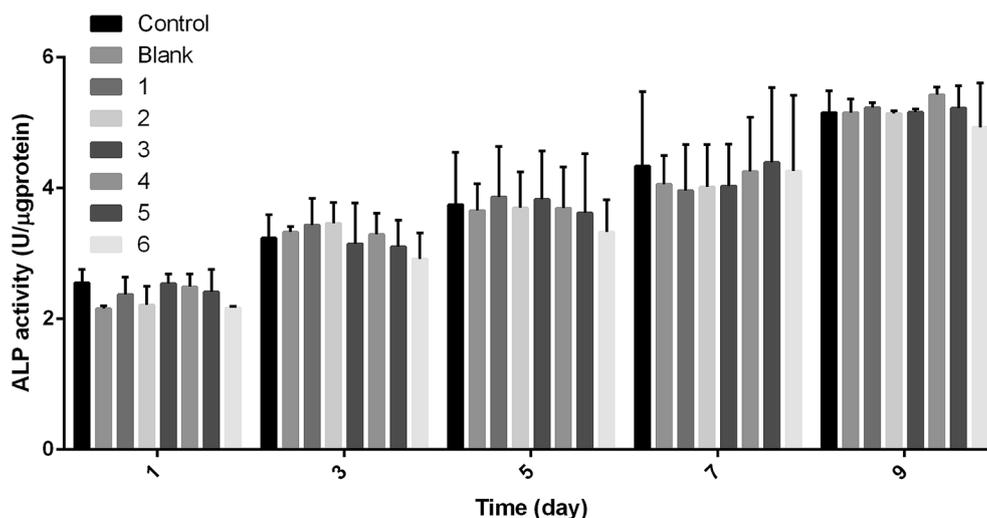


**Fig. 16** Differentiation of MC3T3-E1 on PEEK and PEEK/ZnO composite membranes after 1, 3, 5, 7, and 9 days of cell culture (*$P < 0.05$), blank: PEEK, 1: PEEK/2.5 wt% ZnO, 2: PEEK/5.0 wt% ZnO, 3: PEEK/2.5 wt% m-ZnO, 4: PEEK/5.0 wt% m-ZnO, 5: PEEK/7.5 wt% m-ZnO, 6: PEEK/10 wt% m-ZnO.

**Table 7** Comparison of differences between blank 1, 2, 3, 4, 5, and 6 groups and control (*P* value)

| Time (day) | Control vs. blank | Control vs. 1 | Control vs. 2 | Control vs. 3 | Control vs. 4 | Control vs. 5 | Control vs. 6 |
|---|---|---|---|---|---|---|---|
| 1 | 0.059 | 0.332 | 0.071 | 0.934 | 0.725 | 0.447 | 0.057 |
| 3 | 0.772 | 0.539 | 0.491 | 0.793 | 0.858 | 0.686 | 0.338 |
| 5 | 0.883 | 0.833 | 0.936 | 0.89 | 0.93 | 0.827 | 0.464 |
| 7 | 0.701 | 0.609 | 0.662 | 0.677 | 0.907 | 0.941 | 0.919 |
| 9 | 1.000 | 0.762 | 0.957 | 0.987 | 0.297 | 0.792 | 0.386 |

membrane in the overall trend. From the *P* value in the Table 7, we could find that the differences between six groups and control group were not significant ($P > 0.05$), while the overall significance trend between the control group and the sixth group is higher than the other groups according to the Fig. 16 and the Table 7. Therefore, the results indicated that the sixth group has a greater impact on cell differentiation.

## Conclusions

In summary, PEEK/ZnO nanocomposites were synthesized by conventional melt-blending and compression molding. ZnO nanoparticles in the PEEK matrix and their effects on the properties of PEEK/ZnO nanocomposites were investigated. The results showed that the surface treatment of ZnO influenced the performance of nanocomposites significantly. SEM analyses revealed a good distribution of the nanoparticles within the matrix, showing finer dispersion for samples with lower m-ZnO contents, whereas the unmodified ZnO nanoparticles exhibited considerable aggregation. The distribution of ZnO nano-particles inside the PEEK matrix and the interfacial interaction between the nanoparticles and the PEEK matrix improved when ZnO was modified by APTES. This improvement resulted in enhanced mechanical properties of the nanocomposites. The performance of the nanocomposites is also related to the amount of modified ZnO added, and it's appropriate amount was 5.0–7.5 wt%. The thermal and tribological properties of PEEK/ZnO composites were studied. DSC thermograms showed that the nanoparticles acted as heterogeneous nucleating agents for PEEK, raising its level of crystallinity, whereas no change in its crystalline structure was detected. TGA experiments indicated a strong rise in the thermal stability of the matrix upon increasing ZnO concentration. *In vitro* culture of MC3T3-E1 showed that the cells could proliferate on both PEEK and PEEK/ZnO composites. Therefore, PEEK/ZnO composites can have great potential as biomaterials for orthopaedic and trauma implants.

## Conflicts of interest

There are no conflicts to declare.

## Acknowledgements

## References

1 X. Hou, Y. Hu, X. Hu and D. Jiang, Poly(ether ether ketone) composites reinforced by graphene oxide and silicon dioxide nanoparticles: mechanical properties and sliding wear behavior, *High Perform. Polym.*, 2017, **30**(4), 406–417.

2 T. J. Hoskins, K. D. Dearn, Y. K. Chen and S. N. Kukureka, The wear of PEEK in rolling – sliding contact – simulation of polymer gear applications, *Wear*, 2014, **309**, 35–42.

3 F. Li, Y. Hu, X. Hou, X. Hu and D. Jiang, Thermal, mechanical, and tribological properties of short carbon fibers/PEEK composites, *High Perform. Polym.*, 2017, **30**(6), 657–666.

4 N. Amanat, C. Chaminade, J. Grace, *et al.*, Transmission laser welding of amorphous and semi-crystalline poly-ether-ether-ketone for applications in the medical device industry, *Mater. Des.*, 2010, **31**(10), 4823–4830.

5 Y. Hu, X. Hou, X. Hu and D. Jiang, Improvement in the Mechanical and Friction Performance of Poly(ether ether ketone) Composites by Addition of Modificatory Short Carbon Fibers and Zinc Oxide, *High Perform. Polym.*, 2017, **30**(6), 643–656.

6 J. Song, Y. Liu, Z. Liao, S. Wang, R. Tyagi and W. Liu, Wear studies on $ZrO_2$-filled PEEK as coating bearing materials for artificial cervical discs of $Ti_6Al_4V$, *Mater. Sci. Eng., C*, 2016, **69**, 985–994.

7 C. Gao, G. Zhang, T. Wang and Q. Wang, Enhancing the tribological performance of PEEK exposed to water-lubrication by filling goethite (a-FeOOH) nanoparticles, *RSC Adv.*, 2016, **6**, 51247–51256.

8 M. D. Joshi, A. Goyal, S. M. Patil and R. K. Goyal, Tribological and thermal properties of hexagonal boron nitride filled high-performance polymer nanocomposites, *J. Appl. Polym. Sci.*, 2017, DOI: 10.1002/APP.44409.

9 X. Hu, J. Du, Y. Mu, C. Hu, S. Zhang and Z. Jiang, Preparation and optical properties of poly(arylene ether ketone) nanocomposites containing cadmium sulfide nanoparticles, *High Perform. Polym.*, 2016, **28**, 689–696.

10 A. L. Marcomini, B. T. Rego and R. E. Suman Bretas, Improvement of the short-and long-term mechanical properties of injection-molded poly (etheretherketone) and

hydroxyapatite nanocomposites, *J. Appl. Polym. Sci.*, 2017, DOI: 10.1002/APP.44476.

11 S. Zhu, Y. Zhang, Q. Li, L. Wei and S. Guan, Influence of polytetrafluoroethylene (PTFE) content on mechanical and tribological properties of poly(ether ether ketone)/PTFE coatings prepared by electrostatic powder spraying technique, *High Perform. Polym.*, 2015, **27**, 3–9.

12 L. Lin and A. K. Schlarb, Effect of the varied load conditions on the tribological performance and the thermal characteristics of PEEK-based hybrid composites, *Tribol. Int.*, 2016, **101**, 218–225.

13 L. Liu, L. Xiao, X. Zhang, M. Li, Y. Chang, L. Shang and Y. Ao, Improvement of the thermal conductivity and friction performance of poly(ether ether ketone)/carbon fiber laminates by addition of grapheme, *RSC Adv.*, 2015, **5**, 57853–57859.

14 V. Rodriguez, J. Sukumaran, A. K. Schlarb and D. Baets, . Influence of solid lubricants on tribological properties of polyetheretherketone (PEEK), *Tribol. Int.*, 2016, **103**, 45–57.

15 T. Parpaite, F. Sosson, R. Sonnier, L. Clerc and A. Bergeret, Incorporation of elastomer into poly(ether ether ketone): an attempt to improve the damping factor, *High Perform. Polym.*, 2014, **26**, 986–996.

16 M. S. Abu Bakar, P. Cheang and K. A. Khor, Mechanical properties of injection molded hydroxyapatite–polyetheretherketone biocomposites, *Compos. Sci. Technol.*, 2003, **63**, 421–425.

17 M. S. Abu Bakar, P. Cheang and K. A. Khor, Tensile properties and microstructural analysis of spheroidized hydroxyapatite-poly(etheretherketone) biocomposites, *Mater. Sci. Eng., A*, 2003, **345**, 55–63.

18 A. J. Barton, R. D. Sagers and W. G. Pitt, Bacterial adhesion to orthopaedic implant polymers, *J. Biomed. Mater. Res.*, 1996, **30**, 403–410.

19 M. S. Abu Bakar, M. H. W. Cheng, S. M. Tang, S. C. Yu, K. Liao, C. T. Tan, K. A. Khor and P. Cheang, Tensile properties, tension–tension fatigue and biological response of polyetheretherketone–hydroxyapatite composites for load-bearing orthopedic implants, *Biomaterials*, 2003, **24**, 2245–2250.

20 A. J. Barton, R. D. Sagers and W. G. Pitt, Bacterial adhesion to orthopaedic implant polymers, *J. Biomed. Mater. Res.*, 1996, **30**, 403–410.

21 G. F. Hu, R. F. Quan, Y. M. Chen, D. W. Bi, X. S. Jiang, X. F. Li and J. Y. Li, Fabrication, characterization, bioactivity, and biocompatibility of novel mesoporous calcium silicate/polyetheretherketone composites, *RSC Adv.*, 2016, **6**, 57131–57137.

22 J. R. Sarasua and P. M. Remiro, The mechanical behaviour of PEEK short fibre composites, *J. Mater. Sci.*, 1995, **30**, 3501–3508.

23 N. Pace, M. Marinelli and S. Spurio, Technical and histologic analysis of a retrieved carbon fiber-reinforced poly-ether-ether-ketone composite alumina-bearing liner 28 months after implantation, *J. Arthroplasty*, 2008, **23**, 151–155.

24 P. Scolozzi, Maxillofacial reconstruction using polyetheretherketone patient specific implants by "mirroring" computational planning, *Aesthetic Plast. Surg.*, 2012, **36**, 660–665.

25 X. Li, J. He, W. Bian, Z. Li, W. Zhang, D. Li and J. G. Snedeker, A novel silk-based artificial ligament and tricalcium phosphate/polyether ether ketone anchor for anterior cruciate ligament reconstruction–Safety and efficacy in a porcine model, *Acta Biomater.*, 2014, **10**, 3696–3704.

26 L. C. Gabriel, L. C. Timothy, H. M. Christina, *et al.*, Hydroxyapatite whisker-reinforced polyetherketoneketone bone ingrowth scaffolds, *Acta Biomater.*, 2010, **6**, 856–863.

27 K. L. Wong, C. T. Wong, W. C. Liu, *et al.*, Mechanical properties and *in vitro* response of strontium-containing hydroxyapatite/polyetheretherketone composites, *Biomaterials*, 2009, **30**, 3810–3817.

28 M. S. Abu Bakar, P. Cheng and K. A. Khor, Mechanical properties of injection molded hydroxyapatite polyetheretherketone biocomposites, *Compos. Sci. Technol.*, 2003, **63**, 421–425.

29 Z. Zuowan, C. Longzhan and J. Qiang, The application zinc oxide whisker in its polymer composite, *New Chem. Mater.*, 2001, **29**, 45.

30 L. Fei, H. Keao and Y. Fengyuan, An Investigation of the Tribological Properties of Nanometer ZnO filled PTFE, *Lubr. Eng.*, 2000, **6**, 37–40.

31 N. L. Rosi and C. A. Mirkin, Nanostructures in Biodiagnostics, *Chem. Rev.*, 2005, **105**, 1547–1562.

32 O. Yamamoto, Influence of Particle Size on the Antibacterial Activity of Zinc Oxide, *Int. J. Inorg. Mater.*, 2001, **3**, 643–646.

33 A. M. Díez-Pascual and A. L. Díez Vicente, Development of Nanocomposites Reinforced with Carboxylated Poly(Ether Ether Ketone) Grafted to Zinc Oxide with Superior Antibacterial Properties, *ACS Appl. Mater. Interfaces*, 2014, **6**, 3729–3741.

34 A. M. Díez-Pascual, C. Xu and R. Luque, Development and characterization of novel poly(ether ether ketone)/ZnO bionanocomposites, *J. Mater. Chem. B*, 2014, **2**, 3065–3078.

35 N. Impens, P. Van Der Voort and E. F. Vansant, Silylation of micro-, meso-and non-porous oxides: a review, *Microporous Mesoporous Mater.*, 1999, **28**(2), 217–232.

36 C. H. Chiang, H. Ishida and J. L. Koenig, The structure of γ-aminopropyltriethoxysilane on glass surfaces, *J. Colloid Interface Sci.*, 1980, **74**(2), 396–404.

37 E. Ukaji, T. Furusawa, M. Sato, *et al.*, The effect of surface modification with silane coupling agent on suppressing the photo-catalytic activity of fine $TiO_2$ particles as inorganic UV filter, *Appl. Surf. Sci.*, 2007, **254**(2), 563–569.

38 B. Lei, L. Wang, X. Chen and S. -Kyoung Chae, Biomimetic and molecular level-based silicate bioactive glass–gelatin hybrid implants for loading-bearing bone fixation and repair, *J. Mater. Chem. B*, 2013, **1**, 5153–5162.

39 A. M. Díez-Pascual, M. Naffakh, J. M. González-Domínguez, A. Ansón, Y. Martínez-Rubi, M. T. Martinez and M. A. Gómez, High performance PEEK/carbon nanotube composites compatibilized with polysulfones-II. Mechanical and electrical properties, *Carbon*, 2010, **48**, 3500–3511.

40 T. Kashiwagi, F. Du, J. F. Douglas, K. I. Winey, R. H. Harris and J. R. Shields, Nanoparticle networks reduce the flammability of polymer nanocomposites, *Nat. Mater.*, 2005, **4**, 928–933.

41 Z. X. Huang, Z. A. Tang, J. Yu and S. Bai, Thermal conductivity of nanoscale polycrystalline ZnO thin films, *Phys. B*, 2011, **406**, 818–823.

42 P. Guoliang, G. Qiang, T. Aiguo, *et al.*, Mechanical behaviors of Al$_2$O$_3$ nanoparticles reinforced polyetheretherketone, *Mater. Sci. Eng., A*, 2008, **492**, 383–391.

43 M. H. Cho and S. Bahadur, Study of the tribological synergistic effects in nano CuO-filled and fiber-reinforced polyphenylene sulfide composites, *Wear*, 2005, **258**, 835–845.